cells that were initially infected before the initiation of therapy. The ability of replication-competent viruses to persist in a latent form in resting $CD4^+$ T cells is also consistent with the finding that frequencies of latently infected $CD4^+$ T cells did not decrease appreciably with increasing time on HAART. The isolation of replication-competent virus from patients who have responded well to long-term HAART has also been achieved by Wong *et al.* (*25*) and Chun *et al.* (*26*). Whether latently infected $CD4^+$ T cells can be efficiently reactivated to produce virus in vivo is unknown; however, the existence of a small but relatively stable compartment of latently infected cells should be considered in deciding whether treatment should be stopped in patients with no other evidence of residual virus.

REFERENCES AND NOTES

1. M. E. Harper, L. M. Marselle, R. C. Gallo, F. Wong-Staal, *Proc. Natl. Acad. Sci. U.S.A.* **83**, 772 (1986); D. D. Ho, T. Moudgil, M. Alam, *N. Engl. J. Med.* **321**, 1621 (1989); R. W. Coombs *et al.*, *ibid.*, p. 1626; S. M. Schnittman *et al.*, *Science* **245**, 305 (1989); J. Embretson *et al.*, *Nature* **362**, 359 (1993); G. Pantaleo *et al.*, *ibid.*, p. 355; M. Piatak Jr. *et al.*, *Science* **259**, 1749 (1993); J. W. Mellors *et al.*, *ibid.* **272**, 1167 (1996).
2. M. I. Bukrinsky, T. L. Stanwick, M. P. Dempsey, M. Stevenson, *Science* **254**, 423 (1991).
3. X. Wei *et al.*, *Nature* **373**, 117 (1995).
4. D. D. Ho *et al.*, *ibid.*, p. 123.
5. J. M. Coffin, *Science* **267**, 483 (1995).
6. A. S. Perelson, A. U. Neumann, M. Markowitz, J. M. Leonard, D. D. Ho, *ibid.* **271**, 1582 (1996).
7. A. S. Perelson *et al.*, *Nature* **387**, 188 (1997).
8. W. Cavert *et al.*, *Science* **276**, 960 (1997).
9. R. M. Gulick *et al.*, *N. Engl. J. Med.* **337**, 734 (1997).
10. T.-W. Chun *et al.*, *Nature Med.* **1**, 1284 (1995).
11. T.-W. Chun *et al.*, *Nature* **387**, 183 (1997).
12. C. A. Michie, A. McLean, C. Alcock, P. C. Beverley, *ibid.* **360**, 264 (1992); A. R. McLean and C. A. Michie, *Proc. Natl. Acad. Sci. U.S.A.* **92**, 707 (1995).
13. Y. Li *et al.*, *J. Virol.* **66**, 6587 (1992); G. Sanchez, X. Xu, J.-C. Chermann, I. Hirsch, *ibid.* **71**, 2233 (1997).
14. J. K. Wong *et al.*, *Proc. Natl. Acad. Sci. U.S.A.*, in press.
15. H.-J. Stellbrink *et al.*, *AIDS* **11**, 1103 (1997).
16. The frequency of resting $CD4^+$ T cells carrying replication-competent HIV-1 was determined as described (*11*). Briefly, highly purified resting cells were plated in duplicate fivefold serial dilutions beginning at 5×10^6 cells per well in culture medium consisting of RPMI with 10% heat-inactivated fetal bovine serum, penicillin (50 U/ml), streptomycin (50 μg/ml), and 4 mM L-glutamine supplemented with recombinant interleukin-2 (100 U/ml). Resting $CD4^+$ T cells were activated by the addition to each well of highly purified PHA (0.25 μg/ml; Wellcome Diagnostics, Research Triangle Park, NC) and a >10-fold excess of freshly isolated PBMCs from one or more HIV-1 seronegative donors. These PBMCs were inactivated by γ irradiation with 5000 roentgens in a cesium source irradiator and then washed twice. The next day, PHA was removed, and CD8-depleted PBMCs, which had been stimulated with PHA for 3 days, from an HIV-1–negative donor were added to each well. Cultures were fed and split as needed, and freshly prepared CD8-depleted PHA blasts were added on days 7 to 9. Supernatants collected on day 14 were analyzed for p24 antigen by enzyme-linked immunosorbent assay (ELISA). Preculturing purified resting $CD4^+$ T cells before activation did not consistently decrease the infected cell frequencies, indicating that stable, peristent forms of latent virus predominate in these patients.
17. S. S. Patel, A. D. Duby, D. L. Thiele, P. E. Lipsky, *J. Immunol.* **141**, 3726 (1988).
18. D. Finzi and R. F. Siliciano, unpublished data.
19. D. Finzi *et al.*, data not shown.
20. If the initial levels of latently infected cells before treatment are positively correlated with the time on therapy at which a given patient is studied, then the actual decay rate may be more rapid than the rate suggested by a cross-sectional plot of IUPM versus time. However, there is no reason to believe that the initial levels are correlated with time on therapy. The initial levels of latently infected cells before treatment in these patients are unknown. In a previous study (*11*) of untreated patients and patients on nucleoside analog therapy, the frequency of cells carrying persistent, replication-competent forms of virus ranged from 1 to 81 per 10^6 resting $CD4^+$ T cells. The frequency of cells carrying any replication-competent form of virus ranged from 1 to 420 per 10^6 resting $CD4^+$ T cells in the peripheral blood. These values for the frequencies of latently infected cells were not correlated with CD4 count or viral load. Therefore, there is no reason to expect a correlation between the pretreament level of latently infected T cells and the time at which a given patient was evaluated in our study.
21. A. Molla *et al.*, *Nature Med.* **2**, 760 (1996).
22. J. W. Mellors, B. A. Larder, R. F. Schinazi, *Int. Antiviral News* **3**, 8 (1995); J. H. Condra *et al.*, *J. Virol.* **70**, 8270 (1996); J. Eberle *et al.*, *AIDS Res. Hum. Retroviruses* **11**, 671 (1995).
23. Single-letter abbreviations for the amino acid residues are as follows: A, Ala; E, Glu; F, Phe; G, Gly; I, Ile; K, Lys; L, Leu; M, Met; N, Asn; Q, Gln; R, Arg; S, Ser; T, Thr; and V, Val.
24. M. J. Kozal *et al.*, *Nature Med.* **2**, 753 (1996).
25. J. Wong *et al.*, *Science*, this issue.
26. T.-W. Chun *et al.*, *Proc. Natl. Acad. Sci. U.S.A.*, in press.
27. Some of the patients had received antiretroviral therapy with the following drugs before starting a regimen that suppressed viral load to undetectable levels: AZT (patients 1, 2, 4, 7, 10, 13, 14, 15, 18, 21, and 22), zalcitabine (ddC) (patients 4, 10, 12, and 18), didanosine (ddI) (patients 1, 4, and 8), 3TC (patients 1, 2, 4, 6, 7, and 13), d4T (patients 2, 6, 12, and 15), IDV (patient 2), and RTV (patient 9).
28. L. A. Myers, L. J. McQuay, F. B. Hollinger, *J. Clin. Microbiol.* **32**, 732 (1994).

29. We thank J. Keruly, P. Pentz, and C. Raines for coordinating patient recruitment; E. Pritchard and K. Cooper for help with collection of the samples; M. Castro for help with the culture experiments; Y.-H. Kuo for assistance with the statistical analysis, and C. Ignacio for help with resistance genotyping. We express special thanks to the patients who participated in this study. Supported by NIH grants AI28108 and AI23871 (R.F.S.); AI27670, AI38858, and AI36214 (Center for AIDS Research); and AI29164 (D.R.) and by the Research Center for AIDS and HIV Infection of the San Diego Veterans Affairs Medical Center.

6 August 1997; accepted 9 October 1997

Amidation of Bioactive Peptides: The Structure of Peptidylglycine α-Hydroxylating Monooxygenase

Sean T. Prigge, Aparna S. Kolhekar, Betty A. Eipper, Richard E. Mains, L. Mario Amzel*

Many neuropeptides and peptide hormones require amidation at the carboxyl terminus for activity. Peptidylglycine α-amidating monooxygenase (PAM) catalyzes the amidation of these diverse physiological regulators. The amino-terminal domain of the bifunctional PAM protein is a peptidylglycine α-hydroxylating monooxygenase (PHM) with two coppers that cycle through cupric and cuprous oxidation states. The anomalous signal of the endogenous coppers was used to determine the structure of the catalytic core of oxidized rat PHM with and without bound peptide substrate. These structures strongly suggest that the PHM reaction proceeds via activation of substrate by a copper-bound oxygen species. The mechanistic and structural insight gained from the PHM structures can be directly extended to dopamine β-monooxygenase.

Many mammalian bioactive peptide hormones, neurotransmitters, and growth factors have a COOH-terminal carboxamide (*1–4*). Surprisingly, the amide is not generated by an NH_2 transfer, but rather by N-oxidative cleavage of a glycine-extended prohormone (*2*, *3*). One enzyme, peptidylglycine α-amidating monooxygenase (PAM) (E.C. 1.14.17.3), catalyzes the α-amidation of these diverse physiological regulators, many of which are much less active with free carboxylates. Bioactive peptides produced by PAM are distributed widely across vertebrate and invertebrate species (*5*). The critical role of PAM is highlighted by data showing that a null mutation of the PAM gene in *Drosophila* is larval lethal (*6*). In humans, PAM is the target of drug design for diseases ranging from rheumatoid arthritis to cancer.

PAM is a bifunctional enzyme encoded by a complex single-copy gene that is subject to tissue-specific and developmentally regulated alternative splicing (*1-4*, *7–9*). Two independent enzymatic domains—a monooxygenase domain and a lyase domain—cat-

S. T. Prigge and L. M. Amzel, Department of Biophysics and Biophysical Chemistry, Johns Hopkins School of Medicine, Baltimore, MD 21205, USA.
A. S. Kolhekar, B. A. Eipper, R. E. Mains, Departments of Neuroscience and Physiology, Johns Hopkins School of Medicine, Baltimore, MD 21205, USA.

*To whom correspondence should be addressed.

alyze the two sequential reactions required for peptide amidation (Fig. 1). The isolated domains, separated either through endoproteolytic cleavage or through independent expression, retain their enzymatic activities (*2*, *7*, *9*, *10*). The NH_2-terminal domain, peptidylglycine α-hydroxylating monooxygenase (PHM), catalyzes the stereospecific hydroxylation of the glycine α-carbon of peptidylglycine substrates. The second domain, peptidyl-α-hydroxyglycine α-amidating lyase (PAL), is required to generate α-amidated peptide product and glyoxylate. Both enzymatic activities have broad substrate specificity, since peptides with all 20 amino acid amides have been isolated (*1*, *2*, *4*).

The PHM domain is an ascorbate-dependent, colorless monooxygenase containing two coppers (*10*, *11*), each of which carries one electron of the two electrons required for the monooxygenase reaction (*12*). In addition to its intrinsic interest, PHM is mechanistically similar to the enzyme that converts dopamine to norepinephrine, dopamine β-monooxygenase (DBM or dopamine β-hydroxylase) (E.C. 1.14.17.1) (*13*). Furthermore, rat PHM and DBM exhibit 30% sequence identity over a 286-residue region that includes eight conserved cysteines and six conserved Cu ligands (*1*, *10*, *14*). Despite extensive biochemical experiments, the mechanism of PHM and DBM remained elusive, in part due to lack of structural information. Here we report the three-dimensional structure of PHMcc, the catalytic core of oxidized rat PHM (residues 42 to 356), alone and in complex with a peptide substrate (Table 1). In contrast to other dicopper proteins, the coppers in PHMcc are 11 Å apart and do not form a binuclear center.

PHMcc is a prolate ellipsoid of dimensions 55 Å by 45 Å by 25 Å composed of two nine-stranded β-sandwich domains. Each domain is about 150 residues in length and binds one catalytic Cu (Fig. 2). The domains have similar topologies, each containing a common eight-stranded antiparallel jelly-roll motif (*15*). The interiors of both domains are highly hydrophobic and lack any charged residues. In the region of the loop linking strands 10 and 11 (strand numbers are shown in Fig. 2), the two domains are closely associated through a hydrophobic interface that buries about 500 $Å^2$ of surface area from each domain (total area buried, 1014 $Å^2$). The rest of the interface consists of an interdomain space, ~8 Å wide on average, fully accessible to solvent.

The NH_2-terminal domain (domain I) is a β-sandwich of two antiparallel β sheets—one containing four strands and one containing five. Three disulfide bridges help anchor loops to the domain without linking the two β sheets together. In addition, at the side of the domain opposite to the interdomain space, two loops form a short antiparallel β sheet (strands 4 and 8). The β-sandwich of domain II consists of one four-stranded antiparallel β sheet and one five-stranded mixed β sheet. Two disulfide bridges connect strands from one sheet to strands on the other sheet. In addition to the two main sheets, this domain includes two small antiparallel β sheets, each of which contains two strands (strands 14 and 18 and strands 12 and 20).

Domain I binds one active site Cu, CuA (*16*), with three histidines (H107, H108, and H172); the two histidines adjacent in sequence are located at the beginning of strand 5, whereas the third is at the end of strand 9

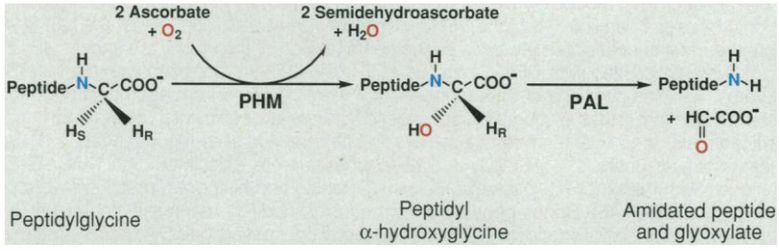

Fig. 1. Reaction catalyzed by bifunctional PAM. The PHM domain catalyzes the oxygen- and ascorbate-dependent hydroxylation of peptidylglycine, forming the α-hydroxyglycine intermediate. The PAL domain cleaves the intermediate and releases amidated peptide and glyoxylate. Colored atoms indicate that molecular oxygen is incorporated into α-hydroxyglycine (*26*), and that the product amide nitrogen is derived from the substrate glycine (*3*).

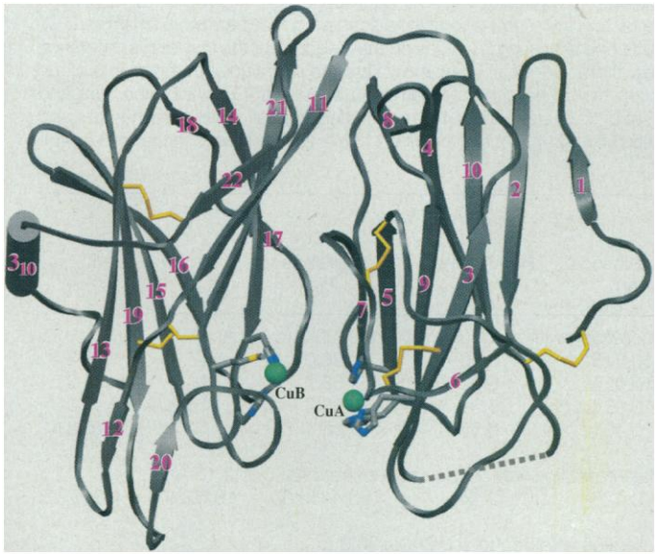

Fig. 2. A representation of the PHMcc fold. The backbone is shown in gray with the coppers represented by green spheres. Strands are numbered arrows and the cylinder is a 3_{10} helix. Side chains of ligands to the two catalytic coppers (green spheres) are colored by atom type (carbon is gray, nitrogen is blue, sulfur is yellow). The dashed gray line indicates a six-residue loop (I176 to D181) not built into the final model. This figure was made with the program Setor (*50*).

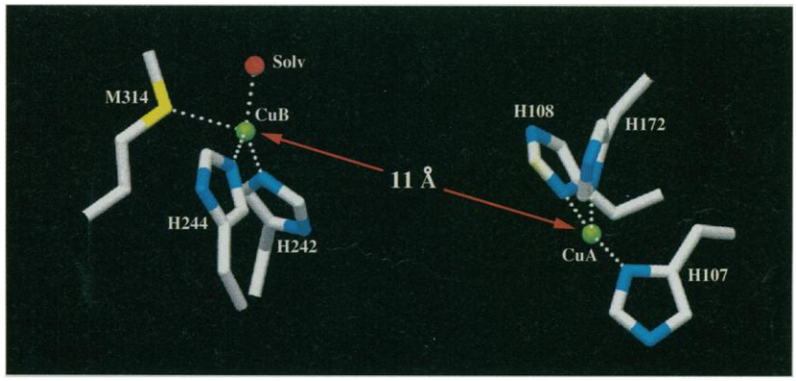

Fig. 3. Coordination geometry of CuA and CuB. Coppers are represented by green spheres and ligands are colored by atom type. Three CuA ligands are shown occupying three of the four equatorial positions of a square pyramidal complex. Four CuB ligands are shown, forming a tetrahedral complex. This figure was made with the program Setor (*50*).

(Fig. 2). Domain II binds the second catalytic Cu, CuB, with two histidines and a methionine (H242, H244, and M314). The histidines are found at the end of strand 14 and the methionine at the beginning of strand 21. All six Cu ligands are conserved among PHM and DBM sequences; mutagenesis of any of these residues eliminates PHM activity (*10*, *17*, *18*).

The two coppers are 11 Å apart and face the interdomain space in such a way that the cleft between them is fully accessible to solvent. The coordination of CuA can be described as square pyramidal with three histidine δ-nitrogens (equatorial) and two unoccupied coordination positions (*19*). The coordination of CuB is tetrahedral, with two histidine ε-nitrogens, one methionine sulfur, and one position occupied by a solvent component, probably a water molecule (this ligand would be displaced by the proposed binding of molecular oxygen to CuB; see below). The solvent ligand departs somewhat from tetrahedral geometry by occupying a position closer to the methionine (Table 2 and Fig. 3).

Previously reported spectroscopic data obtained for oxidized (Cu^{2+}) PHM and DBM are consistent with the coordination of oxidized CuA and CuB observed crystallographically. Extended x-ray absorption fine structure (EXAFS) data support an average of 2.5 N (histidine) and 1.5 O or N ligands per Cu (*10*, *20*, *21*). One study indicated the presence of a weak sulfur ligand at 2.71 Å from CuB in PHM (*10*), in agreement with the 2.68 Å distance observed in the PHMcc structure. X-ray absorption spectroscopy (XAS) data support four-coordinate geometry for the Cu sites in solution, with some evidence for five-coordinate geometry (*20*), in agreement with the CuA and CuB sites observed crystallographically.

In PHM, the CuA site acts as an electron transfer site and the CuB site acts as an oxygen binding site (*10*, *20*). However, structurally, the CuA site is most similar to the oxygen binding sites of other Cu proteins, and the CuB site is most similar to the electron transfer sites of other Cu proteins (*22*). These differences highlight the unusual use of Cu in PHM. In particular, it is surprising that there are open or solvent-occupied coordination positions on both coppers. The coordination of electron transfer sites is typically saturated by protein ligands, and open coordination in the case of CuA may be important for aspects of PHM activity (for example, interaction with ascorbate).

To gain insight into the mechanism of the reaction, we determined the structure of the crystallographically isomorphous complex of PHMcc with *N*-α-acetyl-3,5-diiodotyrosylglycine (*23*) (Table 1 and Fig. 4). Comparison of the structure of oxidized PHMcc with and without bound peptide reveals no significant differences, either in the conformations of individual residues or in the overall structure [0.3 Å root-mean-square (rms) α carbons]. In addition, the CuA-CuB distance is 11 Å in both structures; the binding of peptide does not bring

Table 1. Experimental. The catalytic core (PHMcc) of the monooxygenase domain of rat PAM (residues 42 to 356 of rat PAM-1) was overexpressed in Chinese hamster ovary (CHO) cells through use of the pCIS vector system (*17*, *40*). Crystals of PHMcc were grown by hanging-drop vapor diffusion against transition-metal salts (Ni^{2+}, Co^{2+}, or Cu^{2+}) in buffers ranging from pH 5.25 through pH 8.0 and crystallized in the orthorhombic space group $P2_12_12_1$ with cell dimensions a = 68 Å, b = 69 Å, c = 81 Å, and $\alpha = \beta = \gamma = 90°$ (*41*). Multiple-wavelength anomalous diffraction (MAD) data were collected on three occasions: once at beamline 1-5 of the SSRL (*42*) and twice at beamline X4A of the NSLS (*42*). Statistics from the most successful of the three experiments (at X4A of the NSLS) are shown (*43*). The MAD data sets were processed with DENZO and SCALEPACK (*38*) and analyzed with the MADSYS suite of programs (*44*). The positions of three coppers (*45*) were deduced from anomalous Patterson maps (Patterson maps that have the square of the Bijvoet difference as coefficients) of data from 6 to 2.8 Å. The coordinates and individual temperature factors for the three Cu sites (occupancies = 1) were refined by least-squares analysis in ASLSQ, and MAD phases were calculated with MADABCD—programs included with the MADSYS package. Solvent flattening and histogram matching were performed in the program DM (*46*). Bones generated from density-modified maps skeletonized at 1.5σ were used to identify 17 of the 22 strands in PHMcc and several connecting loops. A partial structure of 222 residues (31 out of register) was built with the program O (*47*) on a Silicon Graphics Indigo2 and used to refine phases in X-PLOR–3.1 (*39*). Refined phases were combined with experimental phases with the program SIGMAA (*46*), improving the map sufficiently to place 247 residues (6 out of register) in 21 strands and again combine phases. From this point on, X-PLOR–3.8 (*39*) was used to refine the structure into a data set collected to 2.0 Å (*48*). The final structure is missing the four NH_2-terminal residues, the three COOH-terminal residues, and a six-residue loop (I176 to D181). This structure was used to phase data collected from a PHMcc-substrate complex (*49*). Data collection statistics: R_{sym} and completeness values were calculated considering Bijvoets equivalent. $R_{sym} = 100 \times \Sigma_h \Sigma_i |I_i(h) - \langle I(h)\rangle| / \Sigma_h \Sigma_i I_i(h)$. MAD structure factor ratios and anomalous scattering factors: $\text{rms}(\Delta|F|)/\text{rms}(|F|)$, where ΔF is the Bijvoet difference at one wavelength (values on the diagonal) or the dispersive difference between two wavelengths (values off the diagonal). Also shown are the anomalous components of the Cu scattering factors as a function of wavelength as determined by MADLSQ (*44*). Refinement and stereochemical statistics: A subset of the data (5 to 8%) was excluded from all steps of refinement and used only for the free R-value calculation (*39*). All data for which $|F| > 3\sigma$ were used in the refinement. $R\text{-value} = \Sigma||F_o| - |F_c|| / \Sigma|F_o|$.

Data collection statistics

Wavelength (Å)	Observations (N)	Redundancy	Completeness (%)	Signal ($\langle I/\sigma I\rangle$)	R_{sym} (%)
MAD data collection without bound substrate (20.0 to 2.3 Å)					
1.3930	110,216	6.90	88.0	17.0	5.2
1.3789	110,925	6.92	88.7	16.4	5.7
1.3779	110,827	6.91	88.3	16.2	6.0
1.3477	110,401	6.88	88.4	14.7	5.8
High-resolution data collection without bound substrate (20.0 to 2.15 Å)*					
1.542	72,425	3.74	90.4 (59.3)	18.6 (3.6)	4.3 (37.2)
Data collection with bound substrate (20.0 to 2.5 Å)*					
1.542	98,056	7.10	99.7 (100.0)	19.1 (4.2)	7.0 (37.0)

MAD structure factor ratios and anomalous scattering factors

λ (Å)	1.3930	1.3789	1.3779	1.3477	f' (e)	f'' (e)
1.3930	0.038	0.040	0.039	0.041	−6.1	0.5
1.3789		0.045	0.036	0.044	−7.9	3.1
1.3779			0.050	0.041	−7.0	3.8
1.3477				0.046	−1.8	3.2

Refinement and stereochemical statistics

	PHMcc without substrate	PHMcc with substrate
Resolution (Å)	6.0 to 2.15	6.0 to 2.5
R value	0.193 ($F > 3\sigma$; 14,759 refl.)	0.197 ($F > 3\sigma$; 11,750 refl.)
Free R value	0.278 ($F > 3\sigma$; 1628 refl.)	0.289 ($F > 3\sigma$; 601 refl.)
Protein atoms	2356	2408
Solvent atoms	162	102
Average B (Å^2)	45.9 (protein), 49.4 (solvent)	44.5 (protein), 40.5 (solvent)
rms deviations		
Bonds (Å)	0.014	0.014
Angles (degrees)	2.090	2.032
Impropers (degrees)	1.421	1.485

*Values in parentheses correspond to the highest resolution shell of data.

the two domains into closer proximity. The positions of structural waters are conserved in both structures, including the water mediating hydrogen bonds between the peptide and PHM. The most significant structural change upon peptide binding is a rotation of the N316 side chain ($\Delta\chi_2 \approx 30°$), breaking a hydrogen bond with Y318 and forming a new hydrogen bond with the backbone of the peptide.

The structure of this complex reveals a binding site tailored to bind peptidylglycine substrates. Several conserved active site residues (R240, Y318, and N316) and one structural water form hydrogen bonds with the peptide backbone of the bound substrate, anchoring it in the interdomain cleft (Fig. 4). In addition, several hydrophobic residues have extensive contact with the substrate, including CuB ligand M314 (*24*). Mutational studies confirm the importance of these interactions. Replacement of Y318 with phenylalanine increases the Michaelis constant (K_m) of PHMcc for peptidylglycine substrate by about sevenfold, with little effect on V_{max} (*17*); and replacement of M314 with isoleucine resulted in an inactive enzyme that bound less tightly to peptidylglycine resin than wild-type PHMcc (*10*).

In reduced DBM, CuB was shown to bind carbon monoxide competitively with respect to oxygen (*21*). In addition, spectroscopic studies with reduced (Cu^+) PHM and DBM found that the sulfur ligand moved closer to CuB (2.27 Å in PHM; 2.25 Å in DBM) than in the oxidized (Cu^{2+}) enzyme (*10*, *21*). Shortening of the sulfur-CuB bond distance upon reduction is probably due to a change of coordination to a ligand geometry favored by Cu^+. The structure of the PHMcc-peptide complex indicates that this geometry would allow peptidylglycine substrates to move closer (by about 0.4 Å) to CuB, because the peptide backbone binds next to the M314 side chain. These results indicate that substrate, oxygen, and CuB are located near each other in the ternary complex with reduced PHM.

The PHM-DBM reaction has been extensively studied, particularly by Klinman and co-workers (*25*). Despite the marked differences in their substrates (peptidylglycine versus dopamine), the reactions catalyzed by PHM and DBM are highly similar. In both cases, a hydroxyl replaces a methylene hydrogen. The enzymatic reactions share the same characteristics: catalytic competence of the reduced enzyme, presence of a radical intermediate, stereospecificity of abstraction (and addition), and incorporation of molecular oxygen into the product (*3*, *4*, *7*, *8*, *12*, *26*, *27*). The crystal structures of PHMcc with and without substrate suggest how events during catalysis occur. The PHM mechanism that results (Fig. 5) combines structural information with salient features of mechanisms proposed for DBM (*28*, *29*).

In the oxidized form of PHMcc (Cu^{2+}), both CuA and CuB are solvent-accessible and may be independently reduced (to Cu^+) by ascorbate in two one-electron reductions (two ascorbates oxidized to two semidehydroascorbates). Molecular oxygen can then bind reversibly to reduced CuB, displacing the solvent ligand. Reversible binding of peptidylglycine substrate takes place as seen in the structure of the PHMcc-substrate complex (Fig. 4): The COOH-terminal oxygens of the peptide form two hydrogen bonds with the guanidinium of R240 and one hydrogen bond

Table 2. Coordination geometry of CuA and CuB. The SOLV ligand could be one N atom of an azide molecule (from the crystallization conditions) instead of water.

Bonds	Å	Angles	Degrees
CuA-H107	1.92	H107-CuA-H108	169*
CuA-H108	2.07	H107-CuA-H172	92†
CuA-H172	2.07	H108-CuA-H172	91†
Bonds	**Å**	**Angles**	**Degrees**
CuB-H242	1.93	H242-CuB-H244	105‡
CuB-H244	2.12	H242-CuB-M314	102‡
CuB-M314	2.68	H242-CuB-SOLV	140‡
CuB-SOLV	2.00	H244-CuB-M314	103‡
		H244-CuB-SOLV	111‡
		M314-CuB-SOLV	80‡

*Ideally 180° for equatorial ligands in square pyramidal geometry. †Ideally 90° for equatorial ligands in square pyramidal geometry. ‡Ideally 109.5° for tetrahedral geometry.

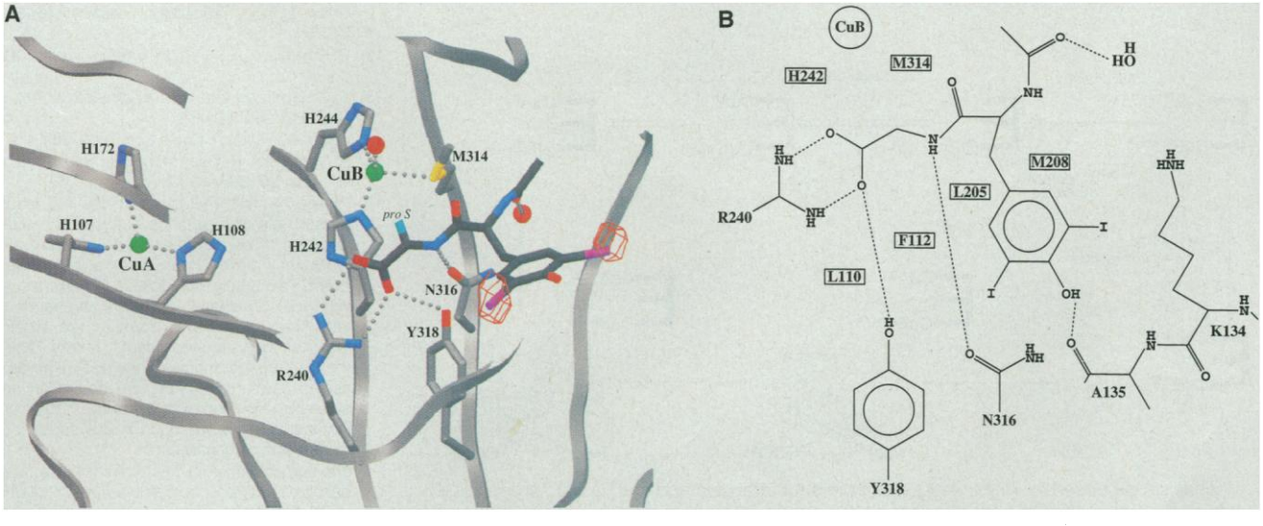

Fig. 4. PHMcc-substrate complex. **(A)** Representation of *N*-α-acetyl-3,5-diiodotyrosylglycine bound in the PHMcc active site. The PHMcc backbone is shown in gray with the coppers represented by green spheres and other atoms colored by atom type. The electron density of a difference (data with and without the substrate are compared) map contoured at 7σ is shown as red mesh, indicating the positions of the electron-dense iodine atoms. **(B)** Contact map depicting residues that interact with bound peptide (within 3.75 Å). Hydrogen bonding interactions and Cu-ligand bonds are indicated with dotted lines. Figure 4A was made with the program Setor (*50*).

with the hydroxyl of Y318. Only in the ternary complex of reduced enzyme, substrate, and molecular oxygen does the reaction progress to produce hydroxylated product, water, and oxidized enzyme (*12*).

In the ternary complex, CuA and CuB transfer one electron each to molecular oxygen, forming peroxide bound to CuB. Hydroperoxide formation requires a proton, yet there are no PHM side chains that can act as a general acid in the vicinity of the Cu-bound peroxide. One possibility is that this proton is provided by the carboxyl of the bound peptide substrate. At physiological pH (pH 5.0 to 5.5 in the subcellular compartments of the neurosecretory pathway) (*30*), the carboxyl of the peptide substrate may be protonated. Binding of the carboxyl to positively charged R240 would lower the pK_a of the carboxylate (where K_a is the acid constant), facilitating transfer of the proton to Cu-bound oxygen. In the peptide-bound structure of PHMcc, the distance between the substrate carboxylate oxygen and CuB is 4.8 Å—well within distance for proton abstraction by a Cu-bound oxygen. This proposal provides a rationale for the required presence of substrate for oxidation of the coppers and explains why peptides terminating in glycylamides (such as oxytocin and vasopressin) are not substrates (*31*).

After hydroperoxide formation, the reaction proceeds as shown in Fig. 5 with heterolytic cleavage of the oxygen-oxygen bond and hydrogen abstraction from the substrate glycine. The resulting glycyl radical then combines with a Cu-bound oxo radical to form a Cu-bound alkoxide product that slowly dissociates. The structure of peptide bound to PHMcc shows how a reaction in which a Cu-bound oxygen species abstracts hydrogen from the α carbon of the substrate glycine can occur. In the structure, the *pro S* hydrogen is pointing toward the CuB site (4.0 Å from CuB) and away from other active site residues. Likewise, the *si* face of the resulting glycyl radical would face the CuB site, ready to react with a Cu-bound oxygen species.

In all mechanisms proposed for PHM and DBM, the two coppers transfer one electron each to molecular oxygen. In other systems (enzyme or biomimetic) where electrons are transferred from more than one Cu to one oxygen molecule, the oxygen is bound bridging two coppers (binuclear center), or the coppers are located close enough for metal-to-metal electron transfer (*32*, *33*). In the case of PHMcc, the coppers are not only distant (11 Å), but the environments around the coppers are not in direct contact with each other. The shortest through-bond electron transfer pathway is 70 residues in length; the shortest pathway involving hydrogen-bonded residues is also prohibitively long (24 residues).

Interdomain motion between domain I and domain II may bring residues near CuA and CuB close enough for electron transfer to occur directly through interdomain contacts (*34*). Such interdomain motion would have to occur in the reduced state, because the structures reported here show that binding of substrate in the presence of oxygen does not alter oxidized PHMcc structure. It is apparent from spectroscopy that interdomain motion does not allow formation of a binuclear Cu center in either oxidation state of PHM or DBM (*10*, *20*, *29*, *35*). Consistent with these findings, if domain I is manually reoriented to form a binuclear center (CuA-CuB = 4.5 Å), the CuA ligand H108 clashes with the substrate glycine, pushing it out of the active site. Alternatively, electron transfer may occur through water molecules in the solvent region between the two domains. The possibility of intramolecular electron transfer through water is intriguing in light of the debate about water as a transfer medium (*36*).

The structures of PHMcc with and without peptide substrate suggest a reaction mechanism in which the enzyme is a scaffold for Cu chemistry. Lack of specific contacts between the enzyme and side chains of the peptide provides a rationale for the broad substrate specificity. Thus, the only function of PHM residues is to provide the coordination of the coppers and to anchor the substrate through hydrogen bonding contacts to its peptide main chain. Significant structural rearrangements would be necessary for additional residues to participate directly in the reaction. The close similarity between the two structures described here argues against this possibility.

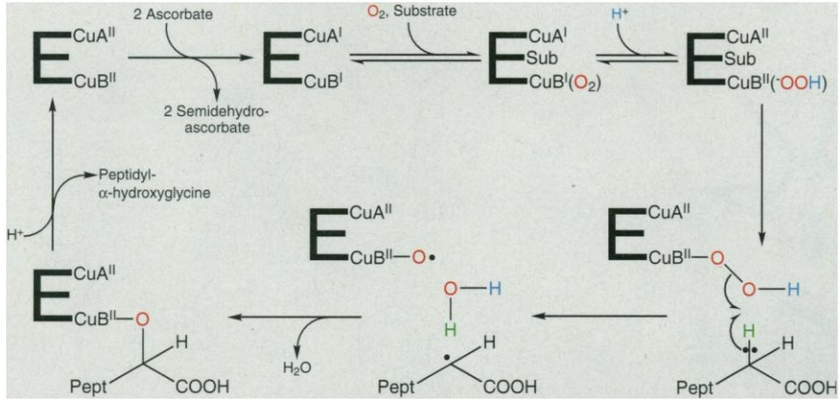

Fig. 5. Mechanism proposed for PHM, developed from structural data and mechanistic proposals (*28*, *29*). Ascorbate reduces both active site coppers. Molecular oxygen binds to CuB reversibly and peptide substrate binds reversibly nearby. Molecular oxygen is then protonated, with the concomitant oxidation of both coppers to Cu^{2+}. The resulting CuB-bound hydroperoxide undergoes heterolytic cleavage of the oxygen-oxygen bond coupled with abstraction of the *pro S* hydrogen of peptidylglycine substrate. The substrate radical combines with the Cu^{2+}-bound oxo radical, forming a Cu^{2+}-alkoxide complex, which then undergoes slow dissociation through protonation from solvent to yield free enzyme and product.

REFERENCES AND NOTES

1. B. A. Eipper, D. A. Stoffers, R. E. Mains, *Annu. Rev. Neurosci.* **15**, 57 (1992).
2. B. A. Eipper, S. L. Milgram, E. J. Husten, H.-Y. Yun, R. E. Mains, *Protein Sci.* **2**, 489 (1993).
3. A. F. Bradbury and D. G. Smyth, *Trends Biochem. Sci.* **16**, 112 (1991).
4. D. J. Merkler, *Enzyme Microb. Technol.* **16**, 450 (1994).
5. In Cnidarians (coral, jellyfish, sea anemones), the lowest animal group having a nervous system, most of the neurotransmitters identified are amidated peptides, suggesting that archetypal nervous systems may have relied on amidated peptides [C. J. P. Grimmelikhuijzen, I. Leviev, K. Carstensen, *Int. Rev. Cytol.* **167**, 37 (1996)].
6. A. S. Kolhekar *et al.*, *J. Neurosci.* **17**, 1363 (1997).
7. A. G. Katopodis and S. W. May, *Biochemistry* **29**, 4541 (1990).
8. M. Noguchi *et al.*, *Biochem. J.* **283**, 883 (1992).
9. K. Suzuki, M. Ohta, M. Okamoto, Y. Nishikawa, *Eur. J. Biochem.* **213**, 93 (1993).
10. B. A. Eipper, A. S. W. Quon, R. E. Mains, J. S. Boswell, N. J. Blackburn, *Biochemistry* **34**, 2857 (1995).
11. R. Kulathila *et al.*, *Arch. Biochem. Biophys.* **311**, 191 (1994).
12. J. C. Freeman and J. J. Villafranca, *J. Am. Chem. Soc.* **115**, 4923 (1993).
13. C. Southan and L. I. Kruse, *FEBS Lett.* **255**, 116 (1989).
14. A. McMahon, R. Geertman, E. L. Sabban, *J. Neurosci. Res.* **25**, 395 (1990).
15. When the two PHMcc domains are structurally aligned, the rms distance between 86 residues (α carbons) of each domain is 1.5 Å, indicating that PHM may have arisen from a gene-duplication event. Two β bulges in domain I (in strands 4 and 7) align with β bulges in domain II (in strands 14 and 16). Although the two domains are topologically identical, their sequence identity is only 4%; none of the disulfide-forming cysteines or Cu ligands is conserved, and the coppers are bound on opposite sides of the β-sandwich domains. Domains with this jelly-roll topology are found in viral capsid proteins, lectins, and glucanases.
16. The nomenclature for the two active site coppers is based on spectroscopic studies (*20*, *21*) of PHM and DBM. In both enzymes, one of the coppers (designated CuB) has a sulfur ligand, whereas the other (CuA) does not.
17. A. S. Kolhekar, H. T. Keutmann, R. E. Mains, A. S. W. Quon, B. A. Eipper, *Biochemistry* **36**, 10901 (1997).
18. H. Yonekura *et al.*, *Biochem. Biophys. Res. Commun.* **218**, 495 (1996).

19. The coordination geometry of CuA is also consistent with square planar geometry, but absorption edge features strongly associated with square planar geometry are absent in XAS data from oxidized PHM (*20*).
20. J. S. Boswell, B. J. Reedy, R. Kulathila, D. Merkler, N. J. Blackburn, *Biochemistry* **35**, 12241 (1996).
21. B. J. Reedy and N. J. Blackburn, *J. Am. Chem. Soc.* **116**, 1924 (1994).
22. The coordination of CuA may include two solvent ligands, in addition to the three histidines. Many proteins in the Protein Data Bank [T. Bernstein *et al.*, *J. Mol. Biol.* **112**, 535 (1977)] contain Cu binding sites composed solely of histidine and solvent ligands (for example, Cu or Zn superoxide dismutase, ascorbate oxidase, and hemocyanin). All of these Cu sites are molecular oxygen acceptors, either for oxidoreductase activity or oxygen transport. The coordination of CuB is most similar to type I Cu sites, which are typically composed of two histidines, one methionine, and one cysteine (for example, cupredoxins, ascorbate oxidase, ceruloplasmin, and Cu nitrite reductase). Type I Cu sites function as electron transfer sites. As observed in PHMcc, the bond length of the Cu-methionine bond in type I Cu sites is long (2.4 to 3.4 Å).
23. This iodinated tyrosylglycine is an effective substrate of PHMcc ($K_m \approx 3$ μM).
24. EXAFS experiments with reduced, anaerobic PAM found that M314 became more rigid (lower Debye-Waller factor) upon binding of peptidylglycine substrate (*20*).
25. J. P. Klinman, *Chem. Rev.* **96**, 2541 (1996).
26. T. M. Zabriskie, H. Cheng, J. C. Vederas, *J. Chem. Soc. Chem. Commun.*, 571 (1991).
27. D. J. Merkler, R. Kulathila, D. E. Ash, *Arch. Biochem. Biophys.* **317**, 93 (1995); J. S. Kizer *et al.*, *Endocrinology* **25**, 2262 (1986); S. E. Ramer, H. Cheng, M. M. Palcic, J. C. Vederas, *J. Am. Chem. Soc.* **110**, 8526 (1988); D. Ping, A. G. Katopodis, S. W. May, *ibid.* **114**, 3998 (1992); P. F. Fitzpatrick and J. J. Villafranca, *J. Biol. Chem.* **261**, 4510 (1986); A. R. Battersby, P. W. Sheldrake, J. Staunton, D. C. Williams, *J. Chem. Soc. Perkin* **I**, 1056 (1976).
28. S. M. Miller and J. P. Klinman, *Biochemistry* **24**, 2114 (1985).
29. M. C. Brenner and J. P. Klinman, *ibid.* **28**, 4664 (1989).
30. This pH corresponds to the pH optimum of rat PHM (*2*, *7*) and also is the pH of the crystallization buffers used for the structures described in this work.
31. Failure of glycylamides to be substrates cannot be attributed to loss of the substrate–R240 salt bridge. Mutation of R240 to glutamine in PHMcc yields an active enzyme with a 2-fold increase in K_m and a 200-fold decrease in V_{max} (*37*). R240 is conserved among PHM sequences; in DBM sequences, R240 is replaced by a conserved glutamine.
32. E. I. Solomon, U. M. Sundaram, T. E. Machonkin, *Chem. Rev.* **96**, 2563 (1996).
33. K. D. Karlin, *Science* **261**, 701 (1993).
34. Crude modeling indicates that interdomain motion in PHMcc could be of two types: hinge motion and shear motion. Hinge motion brings CuA and CuB no closer than 8 Å, but creates new interdomain contacts that may facilitate electron transfer. Shear motion is required to further reduce the distance between CuA and CuB, but in doing so, the interdomain interfaces become increasingly mismatched.
35. R. A. Scott, R. J. Sullivan, W. E. DeWolf Jr., R. E. Dolle, L. I. Kruse, *Biochemistry* **27**, 5411 (1988).
36. M. D. Newton, *J. Electroanal. Chem.* **5025**, 1 (1997); *Chem. Rev.* **91**, 767 (1991).
37. S. T. Prigge, A. S. Kolhekar, B. A. Eipper, R. E. Mains, L. M. Amzel, data not shown.
38. Z. Otwinowski, in *Data Collection and Processing*, L. Sawyer, N. Isaacs, S. Bailey, Eds. (Science and Engineering Research Council, Daresbury Laboratory, Warrington, UK, 1993), pp. 56–62.
39. A. T. Brünger, *X-PLOR, Version 3.1: A System for X-ray Crystallography and NMR* (Yale Univ. Press, New Haven, CT, 1992).
40. Cells were grown in an atmosphere of 5% CO_2 at 37°C in 2-liter roller bottles in 250 ml of α-MEM (minimum essential medium) with 10% fetal calf serum. Six roller bottles were used to produce PHMcc; the most successful culture was harvested for 60 days and produced over 0.75 mg of PHMcc per day during peak production. PHMcc was purified in batches of 4 to 6 liters with three main steps: $(NH_4)_2SO_4$ precipitation, FPLC (fast-protein liquid chromatography) Phenylsuperose chromatography, and FPLC MonoQ chromatography (*10*). Concentration yielded 1.5 ml of PHMcc solution that was >95% pure on the basis of Coomassie brilliant blue staining of SDS-polycrylamide gels and had an absorbance at 280 nm (A_{280}) of 20 units.
41. Crystallization conditions of 525 μM cupric sulfate, 3.08 mM NaN_3, 100 mM dimethylarsinic acid (pH 5.5) at 25°C produced crystals of final dimensions 0.4 mm by 0.1 mm by 0.1 mm over 2 to 4 weeks. Crystals were enlarged to dimensions of 0.8 mm by 0.2 mm by 0.2 mm through macroseeding.
42. Beamline X4A at the National Synchrotron Light Source (NSLS), a U.S. Department of Energy (DOE) facility, is supported by the Howard Hughes Medical Institute. The Stanford Synchrotron Radiation Laboratory (SSRL) is funded by the DOE, Office of Basic Energy Sciences. The Biotechnology Program is supported by the NIH, Biomedical Research Technology Program, Division of Research Resources. Further support is provided by the DOE, Office of Health and Environmental Research.
43. Diffraction data were collected on Fuji HR-5 phosphorimaging plates and digitized with a Fuji offline scanner. Data were collected from a single crystal cryopreserved in buffer [200 μM $CuSO_4$, 100 mM dimethylarsinic acid, 30% (v/v) glycerol] and flash frozen in a 1-mm loop of 11 gauge ethylon surgical fiber in a stream of nitrogen gas (100 K). Four data sets were collected at different x-ray energies at or near the K absorption edge of Cu with the crystal oriented such that Bijvoet pairs could be collected simultaneously. The four data sets were collected in parallel in groups of four 150-s exposures to minimize scaling problems between the data sets.
44. W. A. Hendrickson, *Science* **254**, 51 (1991).
45. The Cu anomalous signal was enhanced by the presence of a third Cu (from the crystallization conditions) at a crystal contact site.
46. Collaborative Computation Project 4, *Acta Crystallogr.* **D50**, 760 (1994).
47. A. T. Jones, J. Y. Zou, S. W. Cowan, M. Kjeldgaard, *ibid.* **A47**, 110 (1991).
48. High-resolution data were collected on an *R*-axis IIc detector with CuKα radiation from a Rigaku RU200 rotating anode and processed in DENZO and SCALEPACK (*38*).
49. The substrate (*N*-α-acetyl-3,5-diiodotyrosylglycine) was synthesized by solid-support peptide synthesis with preiodinated tyrosine (Bachem). The substrate was solubilized at a concentration of 1 mg/ml in 10% glycerol and soaked into a PHMcc crystal for 2 hours before data collection. Diffraction data were collected on an *R*-axis IV detector with CuKα radiation from a Rigaku RU200 rotating anode and processed in DENZO and SCALEPACK (*38*). The PHMcc-substrate complex crystal was isomorphous to native crystals, allowing a difference electron density map ($F_{complex} - F_{native}$) to be calculated with native phases. The substrate iodine positions were deduced from this map contoured at 7σ and the other substrate atoms were built into lower levels of difference density. The PHMcc-substrate structure was refined in X-PLOR–3.8 (*39*) beginning with native phases.
50. S. V. Evans *J. Mol. Graphics* **11**, 268 (1993).

51. We thank C. Ogata and the staff at beamline X-4A for assistance during data collection at the NSLS; H. Bellamy and P. Phizackerly for assistance during data collection at beamline 1-5 at the SSRL; Y. Pan, S. Gabelli, M. Bianchet, K. Lee, G. Bains, M. Faig, D. Medjahed, and K. Doctor for assistance during synchrotron data collection; T. Hand for constructing the R240Q mutant; H. Wu and the Hendrickson group for the MADSYS suite of programs; and D. Leahy, J. Berg, and A. Mildvan for discussions or critical review of this manuscript. Supported by NIH grants DK32949 (B.A.E and R.E.M.) and GM44692 (L.M.A.). The coordinates for PHMcc have been deposited in the Protein Data Bank (accession number 1PHM).

18 August 1997; accepted 7 October 1997

Requirement for the CD95 Receptor-Ligand Pathway in c-Myc–Induced Apoptosis

Anne-Odile Hueber,* Martin Zörnig, Debbie Lyon, Takashi Suda, Shigekazu Nagata, Gerard I. Evan*

Induction of apoptosis by oncogenes like c-*myc* may be important in restraining the emergence of neoplasia. However, the mechanism by which c-*myc* induces apoptosis is unknown. CD95 (also termed Fas or APO-1) is a cell surface transmembrane receptor of the tumor necrosis factor receptor family that activates an intrinsic apoptotic suicide program in cells upon binding either its ligand CD95L or antibody. c-*myc*–induced apoptosis was shown to require interaction on the cell surface between CD95 and its ligand. c-Myc acts downstream of the CD95 receptor by sensitizing cells to the CD95 death signal. Moreover, IGF-I signaling and Bcl-2 suppress c-*myc*–induced apoptosis by also acting downstream of CD95. These findings link two apoptotic pathways previously thought to be independent and establish the dependency of Myc on CD95 signaling for its killing activity.

Most human tumors have genetic alterations in *myc* proto-oncogene family members that result in deregulation of *myc* expression (*1*). However, growth-promoting oncogenes like c-*myc* are also effective inducers of apoptosis, and this lethal attribute may both restrain inappropriate cell growth and maintain normal tissue homeostasis (*2*). Nevertheless, the molecular mechanism by which the c-*myc* gene product, the transcription factor c-Myc, triggers the cell death program remains unknown. In contrast, the mechanism of induction of apoptosis by the transmembrane receptor CD95, which belongs to the tumor necrosis factor (TNF) receptor family, is relatively well characterized (*3*). Upon ligation by its ligand CD95L, a member of the TNF family, CD95 initiates